Magnetic properties and weak ferromagnetism of the dilute antiferromagnets $M_{1-x}Zn_xF_2$ ($M = Mn^{++}, Co^{++}, Ni^{++}$)

A. N. Bazhan and S.V. Petrov

Institute of Physics Problem, USSR Academy of Sciences
(Submitted 14 July 1982)
Zh. Eksp. Teor. Fiz. **84**, 315–334 (January 1983)

The properties of $M_{1-x}Zn_xF_2$ single crystals in magnetic fields up to 65 kOe and at temperatures 2–80 K are studied using a vibrating-reed magnetometer that permits measurements of the three perpendicular components of the sample magnetic moment. At concentrations $0 < x < 0.7$ the $M_{1-x}Zn_xF_2$ samples exhibit properties of the respective MF_2 antiferromagnets in which an increase of x is accompanied by decreases of the Néel temperature T_N, of the effective exchange interaction fields H_E, of the anisotropy fields H_{AE} responsible for orientation of the antiferromagnetic vector **L** relative to the crystal axes, and of the Dzyaloshinskiĭ fields responsible for the transverse ($\sigma_{D\perp}$) and longitudinal ($\sigma_{D\parallel}$) weak ferromagnetism. The phase transitions connected with the rotation of the antiferromagnetic vector **L** in the (001) plane are studied in $Mn_{1-x}Zn_xF_2$ and $Co_{1-x}Zn_xF_2$ at **H**|| [001]. The phase transition from the antiferromagnetic state into a state with transverse weak ferromagnetism $\sigma_{D\perp}$ ||**H** is studied in $Co_{1-x}Zn_xF_2$ at **H**|| [100]. The $Ni_{1-x}Zn_xF_2$ single crystal in the absence of **H** is a weak ferromagnet with transverse weak ferromagnetism. The phase transition due to the onset of longitudinal weak ferromagnetism $\sigma_{D\parallel}$ is studied in $Co_{1-x}Zn_xF_2$ and $Ni_{1-x}Zn_xF_2$ at **H**|| [100].Distinctive properties of dilute antiferromagnet are the growth of the perpendicular magnetic susceptibility in a weak magnetic field when the temperature is lowered to $T < T_N$ and the appearance of a nonlinear $M(H)$ dependence at **H**⊥ [001], likewise in weak magnetic fields H; these are most pronounced when the Zn^{++} concentration x approaches $x_c \approx 0.7$. The distinguishing properties of $Mn_{1-x}Zn_xF_2$ are determined by the appearance of a perpendicular component $\mathbf{m}_\perp^i$ of the magnetic moments $\mathbf{M}_i$ of the M^{++} ions. The component is distributed randomly in the (001) plane and appears and is most pronounced when x approaches x_c.

PACS numbers: 75.50.Ee, 75.30.Et, 75.30.Cr, 75.30.Kz

The antiferromagnetic fluorides Mn^{++}, Co^{++}, and Ni^{++} (MF_2) are among the sufficiently well investigated[1–6] antiferromagnets with $D_{4h}{}^{14}$ tetragonal symmetry (Fig. 1). The MF_2 unit cell contains two magnetics ions M^{++} in the states (0,0,0) and ($\frac{1}{2},\frac{1}{2},\frac{1}{2}$) of the lattice. The fluorides MnF_2 and CoF_2 go over into the antiferromagnetic state at $T < 67$ and $T < 37$ K, respectively, with an antiferromagnetic vector **L** oriented along the tetragonal [001] axis[1,2]; NiF_2 goes over into antiferromagnetic state with weak ferromagnetism $\sigma_{D\perp}$ (Ref. 3) at $T < 73$ K with an antiferromagnetic vector **L** oriented along the binary axes [100] and [010]. In Refs. 1–6 were investigated the static and dynamic (AFMR) properties of these antiferromagnets. Much attention was paid to the investigation of phase transitions in these substances in a magnetic field at different orientations of the applied magnetic field **H** relative to the crystallographic directions. In MnF_2 and CoF_2 were investigated[1,6] phase transitions of the spin-flop type, determined by the flipping of the antiferromagnetic vector **L** when the magnetic field **H** was oriented along the [001] axis. In CoF_2 were investigated[7] transitions from the antiferromagnetic state into a state with transverse weak ferromagnetism $\sigma_{D\perp} \perp$ **L** in a magnetic field oriented along the axis [100] or [010]. In CoF_2 and NiF_2 were investigated phase transitions[8] determined by transverse $\sigma_D \perp$ **L** and longitudinal $\sigma_D \parallel$ **L** weak ferromagnetism at an applied magnetic field orientation **H**|| [110]. The magnetic fields of the phase transitions in these substances, determined by the effective fields of the exchange interaction H_E, of the anisotropy H_A responsible for the orientation of the antiferromagnetic vector **L**, and of the Dzyaloshinskiĭ interaction $H_{D\perp}$ and $H_{D\parallel}$ responsible for the onset of weak ferromagnetism $\sigma_{D\perp}$ and $\sigma_{D\parallel}$, turned out to be quite appreciable (> 100 kOe). In an investigation of the magnetic properties of the dilute antiferromagnet $Mn_{1-x}Zn_xF_2$ we have shown[9] that the values of the effective fields H_E of the exchange interaction and H_A of the uniaxial anisotropy decrease with increasing concentration of the Zn^{++} ions, and at the same time the phase-transition field connected with the flipping of the electromagnetic vector **L** at **H**|| [001] also decreases. It is of interest to investigate phase transitions connected with weak ferromagnetism $\sigma_{D\perp}$ and $\sigma_{D\parallel}$ in single-crystal samples of $M_{1-x}Zn_xF_2$ at different orientations of **H**. In Ref. 10 we have shown that lowering the effective fields H_E and H_A in $Co_{0,5}Zn_{0,5}F_2$ leads also to a lowering of the field of the phase transition from the antiferromagnetic state into state with weak ferromagnetism at **H**|| [100]. In addition to the investigation of the phase transitions in dilute antiferromagnets $M_{1-x}Zn_xF_2$, it is of interest to study the properties of the magnetic state that is produced in these substances when the concentration of the Zn^{++} ion is changed.[11,12] In the investigated fluorides $M_{1-x}Zn_xF_2$, a random replacement of the magnetic ion M^{++} by the magnetic ion Zn^{++} takes place. In this case a random redistribution of the magnetic ions M^{++} takes place in the crystallographic lattice of Fig. 1 in

 0038-5646/83/010181-12$04.00

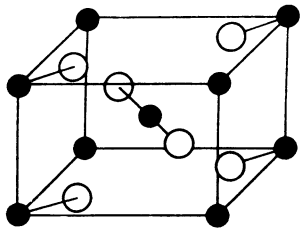

FIG. 1. Unit cell of $M_{1-x}Zn_xF_2$ ($M = M^{++}, Co^{++}, Ni^{++}$): ●–$M^{++}$, Zn^{++}; O–F^-

the positions (0,0,0) and $(\frac{1}{2},\frac{1}{2},\frac{1}{2})$. As shown in Refs. 10—13, at such a distribution of the magnetic ions in $Mn_{1-x}Zn_xF_2$, a state is produced with a randomly distributed component $\mathbf{m}_\perp^i$ of the magnetic moment $\mathbf{M}_i$ of the Mn^{++} ions in the (001) plane, and in addition to the usual properties of the MnF_2 antiferromagnet, $Mn_{1-x}Zn_xF_2$ has also a distinguishing property in that the transverse magnetic susceptibility $\chi_\perp^*$ increases in weak magnetic fields $H \to 0$ when the temperature is lowered, $T < T_N$. It is of interest to study in greater detail this property in $Mn_{1-x}Zn_xF_2$ and to investigate it in $Co_{1-x}Zn_xF_2$ and $Ni_{1-x}Zn_xF_2$.

Our purpose was to investigate the dependences of the magnetic moment of crystalline samples of $M_{1-x}Zn_xF_2$ ($M = Mn^{++}, Co^{++}, Ni^{++}$) on the applied magnetic field at different orientation of **H** relative to the crystal axes and a comparison of the static magnetic properties of the investigated compounds with the corresponding properties of MF_2.

The experiments were performed with a magnetometer with vibrating sample,[14] which made it possible to measure the three mutually perpendicular components of the magnetic moments of the sample in magnetic fields up to 65 kOe and at temperatures from 2 to 80 K. The $M_{1-x}Zn_xF_2$ single-crystal samples were oriented using the x-ray facility of the Institute of Physics problems of the USSR Academy of Sciences. The orientation of the single-crystal axes was accurate to 2–3°. The accuracy with which the percentages of the magnetic and nonmagnetic ions in the investigated compounds were determined was not worse than 10%.

All the samples were prepared by fusing fluorides previously melted and sintered or sublimated in an HF atmosphere. The $Mn_{1-x}Zn_xF_2$ crystals were grown in a helium atmosphere.[9] Owing to the high volatility of the components, the single crystals of the refractory alloys $Co_{1-x}Zn_xF_2$ with high CoF_2 content were grown in sealed platinum crucibles using the apparatus described in Ref. 15. The $Ni_{1-x}Zn_xF_2$ ($x = 0.1$; 0.5) single crystals were obtained by fusing the components in a welded-tight platinum ampoule[16] ~1280° C, followed by slow cooling and subsequent annealing at $T \sim 800°$ C. An x-ray phase analysis of the obtained samples has shown that they are solid solutions.

The concentration of the Zn^{++} ions in the investigated $M_{1-x}Zn_xF_2$ samples was set by the initial contents of the components MF_2 and ZnF_2 during the growth of the same crystals and was checked against the change of the magnetic susceptibility

$$\chi(T) = Ng^2\mu^2 S(S+1)/k(T-\theta),$$

measured at temperatures $T > T_N$ in the paramagnetic region.

EXPERIMENTAL RESULTS

To described the experimental results of the investigation of the magnetization of single-crystal $M_{1-x}Zn_xF_2$, we introduce the following notation: $M_x(H_x)$ is the magnetic moment measured along the applied magnetic field in the X direction, while $M_y(H_x)$ and $M_z(H_x)$ are the magnetic moments measured perpendicular to the applied magnetic field along the Y and Z directions.

Figure 2a shows plots of the magnetic moment $M_x(H_x)$ of the single crystal $Mn_{1-x}Zn_xF_2$ ($x = 0.46$) vs the applied magnetic field at various orientations of **H** relative to the crystal axes. Figure 2b shows for comparison $M_x(H_x)$ plots obtained for MnF_2, in Ref. 1. Figure 2c shows the dependence of the magnetic moment $M_y(H_x)$ with **H** at a small angle ψ to the tetragonal axis [001] (curves 2–4) and along the binary axis [100] (curve 1). It can be seen from Fig. 2a that when the applied magnetic field **H** is oriented along the bina-

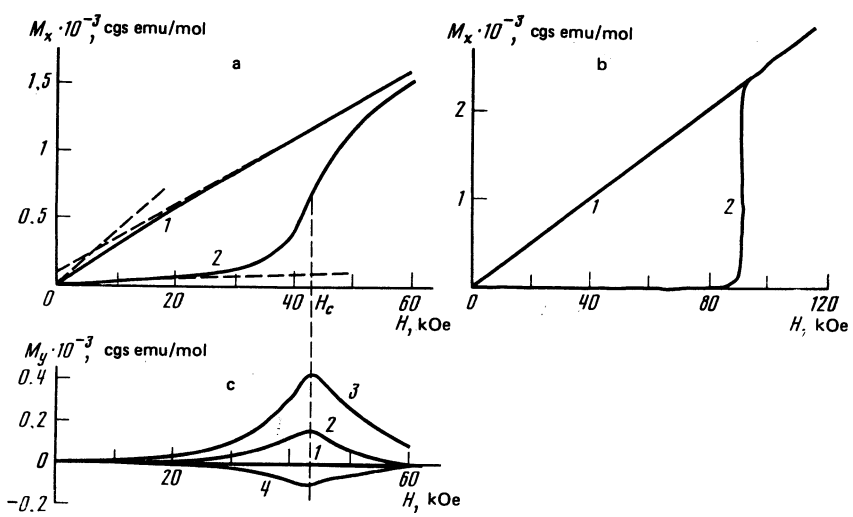

FIG. 2. a) Dependence of the magnetic moment $M_x(H_x)$ of single-crystal $MN_{1-x}Zn_xF_2$ ($x = 0.46$) on the applied magnetic field **H**|| [100]—curve 1, **H**|| [001]—curve 2 b) dependence of $M_x(H_x)$ for MnF_2 at **H**|| [100]—curve 1 and **H**|| [001]—curve 2, obtained in Ref. 1. c) Dependences of the magnetic moment $M_y(H_x)$ at the orientation **H**|| [100]—curve 1 and at orientation of **H** at angles $\pm 1°$ and 2° to the [001] axis (curves 2, 4, and 3, respectively).

ry [100] axis (curve 1), in weak magnetic fields $H < 5$ kOe, one observes in $Mn_{0.54}Zn_{0.46}F_2$, in contrast to MnF_2, a small nonlinear dependence of the magnetic moment $M_x(H_x)$. In strong magnetic fields $H > 20$ kOe, the $M_x(H_x)$ dependence for $Mn_{0.54}Zn_{0.46}F_2$ can be described by the expression $M_x(H_x) = m_\perp + \chi_\perp H$, where $m_\perp = (110 \pm 30)$ cgs emu/mol and $\chi_\perp = (2.6 \pm 0.2) \times 10^{-2}$ emu/mol. The nonlinear $M_x(H_x)$ dependence $\mathbf{H} \parallel [100]$, as shown in Ref. 9, manifests itself most clearly when the Zn^{++} ion concentration approaches $x = x_c \approx 0.7$, where x_c is the concentration at which no phase transition into the antiferromagnetic state is observed. It can also be seen from Fig. 2a that at an orientation $\mathbf{H} \parallel [001]$ (curve 2) in magnetic fields $\mathbf{H} \approx 40$ kOe one observes an appreciable increase of the magnetic moment $M_x(H_x)$. At magnetic fields $H < 10$ kOe, the $M_x(H_x)$ dependence is described by the linear expression $M_x(H_x) = \chi_\parallel H$, where $\chi_\parallel = (2.3 \pm 0.2)10^{-3}$ cgs emu/mol. In magnetic fields $H > 50$ kOe, the magnetic-moment $M_x(H_x)$ obtained at $\mathbf{H} \parallel [100]$. it can be seen from Fig. 2c (curves 2–4) that in magnetic fields $H < 30$ kOe the magnetic moment $M_y(H_x)$ is close to zero. In magnetic fields $H \approx 40$ kOe, a nonzero magnetic moment $M_y(H_x)$ appears, and with further increase of H it again approaches zero. It can be seen from Figs. 2a–2c that the onset of the magnetic moment $M_y(H_x)$ in magnetic fields $H \approx 40$ kOe is due to the increase of the magnetic moment $M_x(H_x)$. These behaviors of the magnetic moments $M_x(H_x)$ and $M_y(H_x)$ at $\mathbf{H} \parallel [001]$ in magnetic fields $H \approx 40$ kOe characterize a phase transition connected with the rotation of the antiferromagnetism vector from a state with $\mathbf{L} \parallel [001]$ into a state with $\mathbf{L} \perp [001]$. In MnF_2 such a phase transition takes place in magnetic field $H_c \approx 90$ kOe. In contrast to the phase transition in MnF_2, the phase transition in $Mn_{1-x}Zn_xF_2$ takes place in weaker magnetic fields, and not exactly in a definite magnetic field H_c, but is a certain range of magnetic fields. The field H_c of the phase transition in $Mn_{1-x}Zn_xF_2$ was determined by us from the inflection point of the $M_x(H_x)$ magnetization curve and from the maximum of the $M_y(H_x)$ magnetization curves; for the concentration $x = 0.46$ (Figs. 2a–2c) we have $H_c = (42 \pm 2)$ kOe.

Investigating the dependences of the magnetic components $M_x(H_x)$ of the single crystal $Mn_{1-x}Zn_xF_2$ at different temperatures and concentrations x of the nonmagnetic ion Zn^{++}, we have plotted the magnetic susceptibilties $\chi(x,T)$ of the investigated single crystals at various orientations and magnitudes of the applied magnetic field $\mathbf{H}$. Figure 3 shows a plot of the magnetic susceptibility $\chi(T)$ for the single crystal $Mn_{1-x}Zn_xF_2$ ($x = 0.46$). It can be seen from Fig. 3 that a temperatures $T > T_N = (23 \pm 1)$ K a paramagnetic $\chi(T)$ behavior is observed, independent of the orientation of $\mathbf{H}$. With decreasing temperature, $T < T_N$, at the orientation $\mathbf{H} \parallel [001]$ and at low values of the applied magnetic field $H \ll H_e$, the value of $\chi_\parallel(T)$ decreases (curve 1) and tends to zero when the temperatures approach zero. From the maximum of $\chi_\parallel(T)$ we have determined the temperature of the phase transition into the ordered state. An investigation of the magnetic susceptibility $\chi_\perp^*(T)$ at the orientation $\mathbf{H} \parallel [100]$ in weak magnetic fields $1 < H < 3$ kOe (curve 2) has shown that even at $T < T_N$ no singularity whatever is observed in the $\chi_\perp^*(T)$ plot at $T = T_N$, and an increase of $\chi_\perp^*(T)$ is observed when the temperature decreases like $\chi_\perp^*(T) \propto (T - \theta)^{-1}$, where θ is a quantity that depends on the concentration x of the Zn^{++} ions. For the sample $Mn_{1-x}Zn_xF_2$ ($x = 0.46$) the value of θ turned out to be $\theta = (21 \pm 2)$ K. In strong magnetic fields $\mathbf{H} > 20$ kOe the magnetic susceptibility $\chi_\perp(T)$ (curve 3) mesured at $\mathbf{H} \parallel [100]$ does not depend on temperature and corresponds to the antiferromagnetic perpendicular magnetic susceptibility of the sample. Figure 4 shows plots of the points T_N/T_N^0 of the phase transition into the ordered state against the concentration of the nonmagnetic ion Zn^{++} in $Mn_{1-x}Zn_xF_2$, where T_N^0 is the phase-transition temperature of MnF_2. It can be seen from Fig. 4 that when the concentration x of the nonmagnetic ions Zn^{++} approaches the value $x = x_c = 0.7 \pm 0.05$ the temperature T_N of the phase transition into the ordered state tends to zero. In experiments at $x > 0.7$ and $T > 2$ K, no maximum of the magnetic susceptibility $\chi_\parallel(T)$ was observed. The $T_N(x)$ dependence is described sufficiently well by the expression $T_N = AT_N^0(0.7 - x)$, where $A = 1.4 \pm 0.1$. Figure 5a shows the dependence of the perpendicular magnetic susceptibility $\chi_\perp(x)/\chi_\perp(0)$ at $\mathbf{H} \parallel [100]$, obtained in weak ($1 < H < 3$ kOe, squares) and strong ($H > 40$ kOe, circles) magnetic fields as functions of the concentration of the Zn^{++} ions in $Mn_{1-x}Zn_xF_2$ where

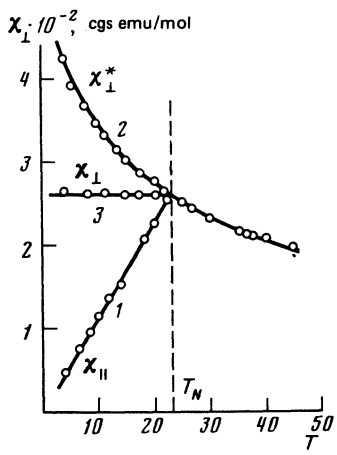

FIG. 3. Dependence of the magnetic susceptibility $\chi(T)$ of the single crystal $Mn_{1-x}Zn_xF_2$, measured in weak magnetic fields at $\mathbf{H} \parallel [001]$— curve 1 and $\mathbf{H} \parallel [001]$— curve 2, and in strong magnetic fields at $\mathbf{H} \parallel [100]$ and $\mathbf{H} \parallel [001]$—curve 3.

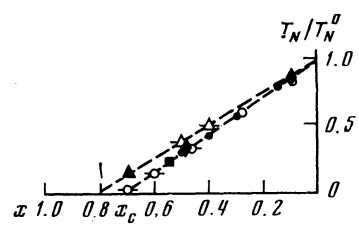

FIG. 4. Dependence of the point of the phase-transition T_N/T_N^0 into the ordered state for $M_{1-x}Zn_xF_2$ single crystals on the Zn^{++} concentration: ○, ●—(Ref. 12), ■—Ref.17—$Mn_{1-x}Zn_xF_2$; △,▲—(Ref. 13)—$Co_{1-x}Zn_xF_2$◇—$Ni_{1-x}Zn_xF_2$

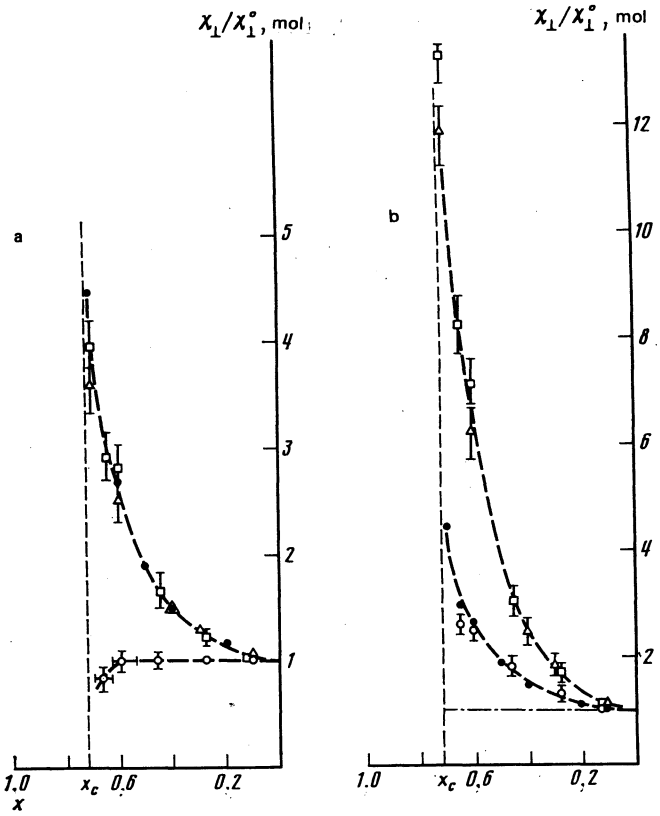

FIG. 5. Dependence of the magnetic susceptibility $(\chi(x)/\chi_\perp(0)$ for $Mn_{1-x}Zn_xF_2$ calculated per mole of material (a) and per Mn^{++} ion (b) and measured H|| [100] in weak magnetic fields (points □), in strong magnetic fields (○) on the concentration of the Zn^{++} ions. The points (◇) designate data obtained in Ref. 11 and the points ● represent the curve calculated in Ref. 20 for a body-centered unit cell.

$\chi_\perp(0)$ is the transverse magnetic susceptibility of MnF_2. In the same figure (triangles) are shown the data obtained in an investigation[11] of the magnetic susceptibility $\chi_\perp(x)$ in magnetic fields $H \approx 5$ kOe. It can be seen from Fig. 5a that with increasing concentration of the Zn^{++} ions the value of $\chi_\perp^*$ increases in weak magnetic fields $1 < H < 3$ kOe. In strong magnetic fields $H > 40$ kOe, the measured magnetic susceptibility $\chi_\perp(x)$ is independent of the concentration of the Zn^{++} ions at $0 < x < 0.5$. When the concentration x approaches 0.7, the magnetic-susceptibility $\chi_\perp^*(x,T)$ obtained in weak magnetic fields increases quite appreciably, and the magnetic susceptibility $\chi_\perp(x)$ obtained in strong fields changes.[1]

We have investigated the magnetization curves $M_x(H_x)$, $M_y(H_x)$, and $M_z(H_x)$ for single crystals of the system $Co_{1-x}Zn_xF_2$. Figure 6a shows plots of the magnetic moment against the applied magnetic field for the single crystal $Co_{1-x}Zn_xF_2$ ($x = 0.5$) at different orientations of **H** relative to the crystallographic directions. Curves 1, 2, and 3 of Fig. 6a the plots of $M_x(H_x)$ at **H**|| [100], **H**|| [110] and **H**|| [001], respectively. Figure 6b shows for comparison the $M_x(H_x)$ plots at **H**|| [100], **H**|| [110] and **H**|| [001] for the single crystal CoF_2, as obtained in Refs. 7 and 8. At the orientation **H**|| [100] in the weak magnetic fields $H < 3$ kOe, a certain nonlinear $M_x(H_x)$ dependence is observed with decreasing magnetic susceptibility, similar to the nonlinear $M_x(H_x)$ dependence for $Mn_{1-x}Zn_xF_2$. In magnetic fields $3 < H < 20$ kOe, the $M_x(H_x)$ dependence is determined by the expression $M_x(H_x) = m_\perp + \chi_\perp^* H$, where $m_\perp = (100 \pm 20)$ cgs emu/mol and $\chi_\perp^* = (6.2 \pm 0.2)10^{-2}$ cgs emu/mol. It must be noted, however, that $m_\perp$ is not large compared with $\chi_\perp^* H$, as will be shown latter, and the function $M_x(H_x)$ at $H < 20$ kOe can be

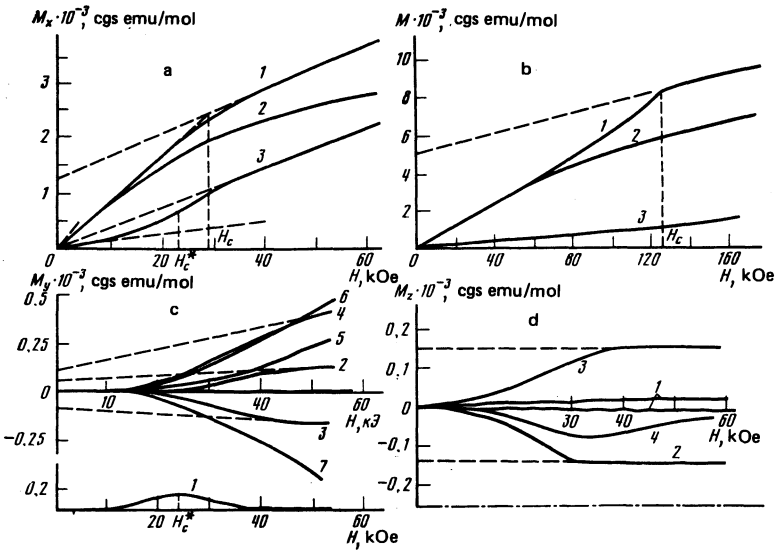

FIG. 6. a—Dependence of the magnetic moment $M_x(H_x)$ on the applied magnetic field for $Co_{1-x}Zn_xF_2$ at **H**|| [100]—curve 1, **H**|| [100]—curve 2, and **H** [001]—curve 3. b—Dependence of $M_x(H_x)$ for CoF_2 at **H**||[100], **H**|| [110] and **H**|| [001]—curves 1, 2, and 3 (Ref. 7), respectively. c—Dependence of the magnetic moment $M_y(H_x)$ for $Co_{1-x}Zn_xF_2$ ($x = 0.5$) with **H** oriented at an angle 1° to the [001] axis—curve 1, at ± 5° to the [100] axis—curves 2 and 3 respectively, at 10° to the [100] axis—curve 4, at 5° to the [110]— curve 5, and at ± 10° to the [110] axis—curves 6 and 7 respectively. d—Dependence of the magnetic moment $M_z(H_x)$ for $Co_{1-x}Zn_xF_2$ at **H**|| [100] and **H**|| [010]—curves 1, and **H**|| [110]—curve 2, at **H**|| [110]—curve 3, and at **H** oriented at an angle 10° to be [110] axis—curve 4.

regarded approximately as linear: $M_x(H_x) = \chi_\perp^* H$. In magnetic fields $H > 30$ kOe, the slope of the magnetization curve $M_x(H_x)$ changes abruptly and $M_x(H_x)$ at $H > 35$ kOe can be described by the expression $M_x(H_x) = \sigma_D + \chi_\perp H$, where $\sigma_D = (1300 \pm 200)$ cgs emu/mol and $\chi_\perp = (2.9 \pm 0.2)10^{-2}$ cgs emu/mol, σ_D being the ferromagnetic moment produced in strong magnetic fields. From the experimental curve on Fig. 6a can be seen that $m_\perp \ll \sigma_D$. In a magnetic field $H < 20$ kOe, oriented along the binary axis [110] (Fig. 6a, curve 2), $M_x(H_x)$ is the same as measured at **H**|| [100] and is described by the expression $M_x(H_x) = \chi_\perp^* H$ where $\chi_\perp^*$ is the quantity indicated above. With increasing magnetic field, at $H > 30$ kOe, the function $M_x(H_x)$ becomes nonlinear and the slope of the magnetization curve $M_x(H_x)$ decreases continuously with increasing H. In a magnetic field oriented along the tetragonal axis [001] (Fig. 6a, curve 3), the plot of $M_x(H_x)$ in weak magnetic fields $H < 10$ kOe is linear and is determined by the expression $M_x(H_x) = \chi_\parallel H$, where $\chi_\parallel = (1 \pm 0.1)10^{-3}$ cgs emu/mol. In magnetic fields $10 < H < 35$ kOe one observes a nonlinear increase of the magnetic moment $M_x(H_x)$ which can be described at $H > 35$ kOe by the relation $M_x(H_x) = \chi_\perp H$, where $\chi_\perp = (2.8 \pm 0.2)\cdot 10^{-2}$ cgs emu/mol is the perpendicular magnetic susceptibility at **H**|| [001]. A comparison of the obtained $M_x(H_x)$ dependences for $Co_{1-x}Zn_xF_2$ with the analogous $M_x(H_x)$ dependence for CoF_2 (Refs. 7,8) shows that in the investigated substance, at an applied magnetic-field orientation **H**|| [100] and in magnetic fields $H < 30$ kOe, a phase transition place from the purely antiferromagnetic state with **L**|| [001] into a state with weak ferromagnetism $\sigma_{D_\perp}$||**H** and an antiferromagnetic vector **L** ⊥ **H**. In a magnetic field $H \approx 24$ kOe, oriented along the tetragonal axis [001], in magnetic a phase transition takes place and is connected with the rotation of the antiferromagnetic vector **L** from the state with **L**|| [001] into the state with **L**⊥ [001]. Similar phase transitions are observed in CoF_2 at $H_c = (120 \pm 5)$ kOe, **H**|| [100] (Refs. 7 and 8), and $H_c^* = (240 \pm 20)$ kOe, **H**|| [001] (Ref. 6). It can thus be concluded that when the magnetic Co^{++} ions are replaced by the nonmagnetic Zn^{++} in the tetragonal CoF_2 lattice the values of the phase-transition fields in $Co_{1-x}Zn_xF_2$, just as in $Mn_{1-x}Zn_xF_2$, decreases. Figures 6c and 6d show plots of the magnetic moments $M_y(H_x)$ and $M_x(H_x)$ at different orientations of **H**. It can be seen that at the orientation **H**|| [001] (Fig. 6c, curve 1) the $M_y(H_x)$ dependence, just as the analogous $M_y(H_x)$ dependence for $Mn_{1-x}Zn_xF_2$ (see Fig. 2c) has in the phase-transition magnetic field H_c^* a value that differs maximally from zero. In weak ($H < 10$ kOe) and strong ($H > 35$ kOe) magnetic fields, $M_y(H_x)$ is close to zero. This character of the dependence of this projection of the magnetic moment on the applied magnetic field also points to a phase transition connected with rotation of the antiferromagnetic vector **L**. When the orientation of the applied magnetic field **H** changes in the (001) plane (Fig. 6c), the resultant nonlinear $M_y(H_x)$ dependences have different properties for **H** oriented near the axes [100] and [110]. In magnetic fields **H**|| [100] and **H**|| [110], $M_y(H_x)$ are close to zero at all values of H. When **H** is oriented close to the [100] axis (Fig. 6c, curves 2–4), the $M_y(H_x)$ dependence in strong magnetic fields $H > 35$ kOe can be described by the expression $M_x(H_x) = \sigma_{D_\perp}(\psi) + \chi_\perp(\psi)H$, where ψ is the angle between the direction of **H** and the [100] axis, and $\sigma_{D_\perp}(\psi)$ and $\chi_\perp(\psi)H$ are the projections of the ferromagnetic and magnetic moments on the measurements axis V. At a magnetic field **H** oriented near the [110] axis, the $M_y(H_x)$ dependence (Fig. 6c, curves 5–7) is nonlinear in the entire range of employed magnetic fields. This dependence determines the onset of $M_y(H_x)$ at a certain complicated rotation of the antiferromagnetic vector **L**. It can be seen from Fig. 6d that in a magnetic field oriented along the binary axis [100] the plots of $M_z(H_x)$ (curves 1) are linear and are close to zero. The slope of the $M_z(H_x)$ plot at certain orientations **H**|| [100] (which repeat every 90°) is determined by the inaccurate orientation of the tetragonal [001] axis relative to the Z axis. The $M_z(H_x)$ dependences for a magnetic field oriented along the [100] axis are of interest. In this case, $M_z(H_x)$ is a nonlinear function in magnetic fields $H < 30$ kOe, and when the magnetic field is increased to $30 < H < 50$ kOe, $M_z(H_x)$ assumes a constant value $M_z(H_x) = \sigma_D^*$, where $\sigma_D^* = (360 \pm 40)$ cgs emu/mol. In magnetic fields $H > 50$ kOe, a small decrease of $M_z(H_x)$ is observed. When the magnetic field makes an angle $\psi \approx 10°$ with the [110] axis, the decrease of $M_z(H_x)$ in strong magnetic fields becomes more pronounced (curve 4 of Fig. 6d).

Investigating the dependences of the magnetic moment on the applied magnetic field at various temperatures, we have plotted the magnetic susceptibility vs. temperature at different orientations and values of the applied magnetic field **H**. These plots are shown in Fig. 7a. Figure 7b shows a plot of the ferromagnetic moment $\sigma_{D_\perp}$ against temperature at an orientation **H**|| [100]; this plot was obtained by extrapolating the magnetization curves $M_x(H_x)$ in strong magnetic fields $H > 30$ kOe to $H = 0$. It can be seen from Fig. 7a that at **H**|| [001] the magnetic susceptibility $\chi_\parallel(T)$ measured in weak magnetic fields $H < 20$ kOe decreases with decreasing temperature to $T < T_N = (12 \pm 1)$K (curve 1). The phase-transition point T_N is determined from the maximum of the $\chi_\parallel(T)$ plot. In strong magnetic fields $H > 35$ kOe the magnetic susceptibility $\chi_\perp$ does not depend on the temperature–curve 2 of Fig. 7a. In a magnetic field oriented along the binary axis [100], in weak magnetic fields $1 < H < 3$ kOe (Fig. 7a, curve

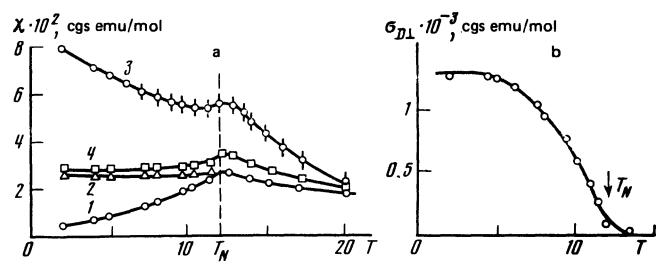

FIG. 7. a—Temperature dependences of the magnetic susceptibility $\chi(T)$ for $Co_{1-x}Zn_xF_2$ measured in weak magnetic yields at **H**|| [001]—curve 1, **H**|| [100]—curve 2, and in strong magnetic fields at **H**|| [001]—curve 3, **H**|| [100]—curve 4. b—Temperature dependence of the magnetic moment $\sigma_{D_\perp}$ of the single crystal $Co_{1-x}Zn_xF_2$.

3), just as under the analogous conditions in the investigation of $Mn_{1-x}Zn_xF_2$ (Fig. 3, curve 2), an increase of the magnetic susceptibility $\chi_\perp^*(T)$ is observed with decreasing temperature $T < T_N$. The distinguishing feature of the $\chi_\perp^*(T)$ dependence for $Co_{1-x}Zn_xF_2$ is the maximum of $\chi_\perp^*(T)$ at the phase-transition point $T = T_N$. The latter, as indicated in Ref. 18, is determined in the investigation of CoF_2 by the induction of magnetic order in the vicinity of $T = T_N$ in crystals subject to the Dzyaloshinskiĭ interaction that causes its weak ferromagnetism $\sigma_{D_\perp}$. In the investigation of the magnetic susceptibility $\chi_\perp(T)$ in magnetic fields $H > 35$ kOe (curve 4 of Fig. 7a) one observes a temperature-independent value of $\chi_\perp$, which also has a maximum $\chi_\perp(T)$ near the phase-transition point T_N. The temperature of the phase transition into the ordered state, determined from the vanishing of the ferromagnetic moment $\sigma_{D_\perp}$ (Fig. 7b), turns out to be $T_N = (12 \pm 1)$ K. Figure 4 shows plots of the phase transition temperature T_N/T_N^0 into the ordered state on the concentration of the Zn^{++} ions in $Co_{1-x}Zn_xF_2$. Marked in the same figure is the T_N/T_N^0 phase transition point $Co_{0.3}Zn_{0.7}F_2$, obtained in Ref. 13. It can be seen from Fig. 4 that the phase transition temperature T_N decreases with increasing x and approaches zero at $x = x_e = 0.8 \pm 0.05$ in accord with the law $T_N = BT_N^0(0.8 - x)$, where $B = 1.2 \pm 0.05$ and T_N^0 is the temperature of the phase transition into CoF_2. Just as in $Mn_{1-x}Zn_xF_2$, one observes in $Co_{1-x}Zn_xF_2$ an increase of the magnetic susceptibility $\chi_\perp^*(x,T)$ obtained in weak magnetic fields $1 < H < 3$ kOe. In strong magnetic fields $H > 35$ kOe one observes for the two $Co_{1-x}Zn_xF_2$ ($x = 0.4;0.5$) samples measured by us, a magnetic susceptibility independent of the concentration x. The increase of the magnetic susceptibility $\chi_\perp^*(x)$ is determined by the strong dependence of $\chi_\perp^*(T)$ on the temperature.

We have also investigated the dependences of the magnetic moment on the applied magnetic field for a single-crystal sample $Ni_{1-x}Zn_xF_2$ ($x = 0.5$). Figure 8a shows plots of $M_x(H_x)$ at orientations $\mathbf{H} \parallel [100]$ and $\mathbf{H} \parallel [110]$. At $\mathbf{H} \parallel [001]$, the $M_x(H_x)$ dependence is linear and it is described by the expression $M_x(H_x) = \chi_\perp H$ where $\chi_\perp = (1.6 \pm 0.2)\cdot 10^{-2}$ cgs emu/mol. In Fig. 8a this dependence is shown by the dashed line 3. In Fig. 8b are shown for comparison the $M_x(H_x)$ dependences for NiF_2 at the same orientations of $\mathbf{H}$ as obtained in Ref. 4. It is seen from Fig. 8a that the orientation of $\mathbf{H}$ along the binary axis [100] the $M_x(H_x)$ dependence for $Ni_{1-x}Zn_xF_2$ in magnetic fields $H > 6$ kOe is described by the expression $M_x(H_x) = \sigma_{D_\perp} + \chi_\perp H$, where $\sigma_{D_\perp} = (120 \pm 10)$ kOe and $\chi_\perp = (1.6 \pm 0.2)\cdot 10^{-2}$ cgs emu/mol. According to this experiment, the single-crystal $Ni_{1-x}Zn_xF_2$ has a weak ferromagnetism $\sigma_{D_\perp}$, and the ferromagnetic moment is directed in this case along the [100] axis of the crystal. At an applied magnetic-field orientation $\mathbf{H}$ along the binary axis [110] (curve 2 of Fig. 8a), in weak magnetic fields H, the $M_x(H_x)$ dependence can be described by the expression $M_x(H_x) = \sigma_D^* + \chi^* H$, where $\sigma_D^* \approx \sqrt{2}\sigma_{D_\perp}/2$ and $\chi^* = \chi_\perp/2$. With increasing magnetic field, a nonlinear increase of the magnetic moment $M_x(H_x)$ is observed and this dependence tends to the one described by the expression $M_x(H_x) = \chi_\perp H$, where $\chi_\perp$ is the magnetic susceptibility of the sample of $\mathbf{H} \parallel [100]$. It can be seen from Fig. 8a that in magnetic fields $H > 55$ kOe the experimental $M_x(H_x)$ dependence at $\mathbf{H} \parallel [110]$ (curve 2) practically coincides with the $M_x(H_x)$ dependence described by the expression $M_x(H_x) = \chi_\perp H$ (curve 3). A comparison of the experiments shown in Figs. 8a and 8b shows that the approach of the magnetic-moment $M_x(H_x)$ dependence at $\mathbf{H} \parallel [110]$ to the $M_x(H_x) = \chi_\perp H$ dependence for the $Ni_{1-x}Zn_xF_2$ sample is much faster than for the NiF_2 sample. Figure 8c shows also the dependence of the magnetic moment $M_y(H_x)$, measured in the basal plane of the $Ni_{1-x}Zn_xF_2$ crystal perpendicular to the applied magnetic field at $\mathbf{H} \parallel [100]$ (curve 1) and at an orientation of $\mathbf{H}$ close (within an angle of the order of 1°) to the [110] axis (curve 2). It can be seen from Fig. 8c that at the orientation $\mathbf{H} \parallel [100]$ in

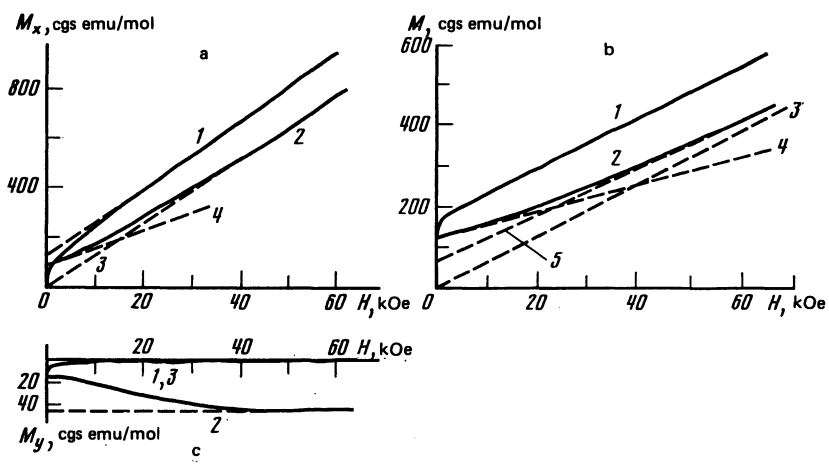

FIG. 8. a—Dependences of the magnetic moment M_x for $Ni_{1-x}Zn_xF_2$ on the applied magnetic field $\mathbf{H} \parallel [100]$—curve 1, $\mathbf{H} \parallel [110]$—curve 2, $\mathbf{H} \parallel [001]$—curve 3. The dashed line 3 represents the $M_x(H_x) = \chi_\perp H$ dependence, curve 4—$M_x(H_x)$ at $\mathbf{H} \parallel [110]$ in weak magnetic fields. b—Plots of $M_x(H_x)$ for NiF_2, obtained in Ref. 4 at $\mathbf{H} \parallel [100]$ and $\mathbf{H} \parallel [110]$—curves 1 and 2, respectively. The dashed curve 4 is a plot of $M_x(H_x) = \sqrt{2}\sigma_{D_\perp}/2 + \chi_\perp H/2$ in the weak magnetic fields $H < 5$ kOe at $\mathbf{H} \parallel [110]$, curve 5—the function $M_x(H_x)$ at $\mathbf{H} \parallel [110]$ and $\mathbf{H} > 50$ kOe, curve 3—the function $M_x(H_x) = \chi_\perp H$. c—Dependence of the magnetic moment $M_y(H_x)$ for $Ni_{1-x}Zn_xF_2$, measured at $\mathbf{H} \parallel [100]$—curve 1, $\mathbf{H} \parallel [110]$—curve 3, and H oriented at an angle 1–2° to the [110]—curve 2.

weak magnetic fields one observes a certain magnetic moment $M_y(H_x)$, which decreases with increasing magnetic field H and becomes practically equal to zero at $H > 5$ kOe. At exact orientation of the magnetic field $\mathbf{H}\|$ [110]. The $M_y(H_x)$ plot (curve 3 of Fig. 8c) is also close to zero, but if $\mathbf{H}$ is directed at a small angle $\psi \approx 1°$–$2°$ to the [110] axis, a magnetic moment $M_y(H_x)$ is produced (curve 2 in the same figure), which increases linearly with increasing H and tends to a constant value $M_y(H_x) = \sigma_D$, where $\sigma_D = (48 \pm 4)$ cgs emu/mol.

Measurement of $M_x(H_x)$ and $M_y(H_x)$ at diffferent temperatures has shown that the nonlinearity of the magnetic moment $M_x(H_x)$ as a function of the magnetic field at $\mathbf{H}\|$ [110] and the approach of $M_x(H_x)$ to the relation $M_x(H_x) = \chi_\perp(T)H$ manifest themselves most strongly at temperatures $T = 4.2$–8 K. With further rise of temperature of nonlinearity of $M_x(H_x)$ vanishes, and at temperatures $T > 18$ K the magnetization curves $M_x(H_x)$ at $\mathbf{H}\|$ [110] become linear and practically coincide with the magnetization curves at $\mathbf{H}\|$ [100], and are described by the expression $M_x(H_x) = \sigma_D(T) + \chi(T)H$. From the $M(H,T)$ dependences we have plotted the magnetic susceptibility $\chi_\perp(T)$ at $\mathbf{H}\|$ [100] and $\mathbf{H}\|$ [001] (Fig. 9a, curves 1 and 2) and the dependences of the ferromagnetic moments $\sigma_{D_\perp}$ and σ_D (curves 1 and 2, Fig. 9b). The temperature T_N, determined from the vanishing at the ferromagnetic moment $\sigma_{D_\perp}$ at $\mathbf{H}\|$ [100] and from the observed maximum of the magnetic susceptibility $\chi_\perp(T)$ and $\mathbf{H}\|$ [100] turned out, for the investigated $Ni_{1-x}Zn_xF_2$ samples, to be $T_N = (22 \pm 1)$ K. From Fig. 9a it can be seen that the decrease of the value of the ferromagnetic moment $\sigma_D(T)$ with increasing temperature is much faster than the decrease of the ferromagnetic moment $\sigma_{D_\perp}(T)$. At temperatures $T > 18$ K the value of $M_y(H_x) = \sigma_D$ is practically close to zero and the magnetic moment $M_x(H_x)$ is directed along the magnetic field $\mathbf{H}\|$ [110]. It can be seen from Fig. 9a that just as in $Mn_{1-x}Zn_xF_2$ and $Co_{1-x}Zn_xF_2$, the perpendicular magnetic susceptibility $\chi_\perp(T)$ in $Ni_{1-x}Zn_xF_2$ increases with decreasing temperature $T < T_N$. In the vicinity of T_N, a maximum of the magnetic susceptibility $\chi_\perp(T)$ is observed at $\mathbf{H}\|$ [100] and corresponds to the onset of magnetic ordering near the temperature T_N in crystals having a Dzyaloshinskiĭ interaction.[18] It is difficult to say anything concerning the nonlinearity of the magnetization curve $M_x(H_x)$ of $Mn_{1-x}Zn_xF_2$ (see Fig. 2a), since the $M_x(H_x)$ curve for $Ni_{1-x}Zn_xF_2$ in these fields is linear because of the weak ferromagnetism $\sigma_{D_\perp}$.

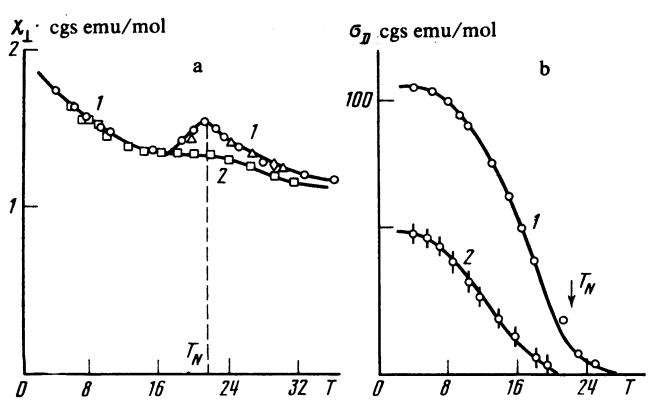

FIG. 9. a—Dependence of the magnetic susceptibility $\chi_\perp(T)$ on the temperature of $Ni_{1-x}Zn_xF_2$, measured at $\mathbf{H}\|$ [100] and $\mathbf{H}\|$ [001]—curves 1 and 2, respectively. b—Dependence of the magnetic moments $\sigma_{D_\perp}(T)$ and $\sigma_{D_\|}(T)$ for $Ni_{1-x}Zn_xF_2$ on the temperature—curves 1 and 2, respectively.

DISCUSSION OF RESULTS

Before we discuss the ordinary antiferromagnetic properties possessed by the $M_{1-x}Zn_xF_2$ systems investigated by us, we consider the properties that distinguish them from pure MF_2. We shall discuss the results under the assumption that in the MF_2 crystal lattice there takes place a random replacement of the magnetic ions M^{++} by the nonmagnetic Zn^{++}.

Distinguishing properties of the investigated randomly diluted systems $M_{1-x}Zn_xF_2$ are the appearance of nonlinearity of the magnetization curve $M_x(H_x)$ in weak magnetic fields when $\mathbf{H}$ is oriented in the (001) plane, and the increase of the magnetic susceptibility $\chi_\perp(T)$ likewise measured in weak magnetic fields when the temperature is lowered below the phase-transition point T_N and when the concentration x of the Zn^{++} ions approaches $x = x_c$. Such as increase of the magnetic susceptibility was observed also in an investigation[19] of the magnetic properties of $KMn_xMg_{1-x}F_2$ and in an investigation[11] of $Mn_{1-x}Zn_xF_2$. We shall explain this result on the basis of the theory developed by A. B. Harris and S. Kirkpatrick,[20] who attribute the nonlinearity of $M_x(H_x)$ and the growth of the dependence of the perpendicular magnetic susceptibility $\chi_\perp^*(x)$ on the concentration of the Zn^{++} ions to the appearance and to the increasing role of ferromagnetic fluctuations of the magnetic moments M_i of the ions M^{++} and to the decrease of the effective number of neighbors of the interacting magnetic ions M^{++}. If account is taken, as is done in Refs. 10 and 20, of only the exchange interaction of the magnetic ions and of the anisotropy responsible for the orientation of the antiferromagnetic vector $\mathbf{L}$ relative to the crystal axes, the Hamiltonian that describes the properties of the dilute antiferromagnet can be written in the form

$$\mathcal{H} = 2J\sum_{ij} p_i p_j S_i S_j - {}^1/_2 K\left[\sum_i p_i (S_i^z)^2 + \sum_j (S_j^z)^2\right] - g\mu H\left[\sum_i p_i S_i^x + p_j S_j^x\right], \quad (1)$$

where $p_i p_j$ is equal to unity if the states (i, j) are occupied by the ions M^{++}, and to zero in all other cases. The quantities J, K, and H represent the exchange interaction of two magnetic ions side by side, the anisotropy of the magnetic ion, and the magnetic field perpendicular to the [001] axis. In the classical case, introducing the angles θ_i and θ_j between the corresponding spin and the easy axis, and putting $g\mu_B H_E = 2JzS$ and $g\mu_B H_A = KS$, where z is the effective number of the nearest interacting M^{++} ions, the Hamiltonian (1) can be rewritten in the form

$$\mathscr{H}/g\mu_B S = H_E \sum_{ij} p_i p_j \cos(\theta_i+\theta_j) - {}^1/_2 H_A \left[\sum_i p_i \cos^2\theta_i + \sum_j p_j \cos^2\theta_j\right] - H_0 \left[\sum_i p_i \sin\theta_i + \sum_j p_j \sin\theta_j\right]. \quad (2)$$

In the equilibrium state $\partial\mathscr{H}/\partial\theta_i = \partial\mathscr{H}/\partial\theta_j = 0$ and it is possible to obtain a system of equations of the form

$$\left[\frac{n_i}{zH_E} + H_A\right]\bar{\theta}_i + \frac{H_E}{z}\sum_j p_j\theta_j - H_0 = 0 \quad (3)$$

(where n_i and z are the number of magnetic ions and the total number of surrounding ions), with which to find the orientations of each spin S_i of the magnetic ion M^{++} relative to the easy axis [001]. As indicated in Refs. 11 and 20, the solution of a system of equations of the form (3) is in the general case difficult. In Refs. 11 and 20 they solved the problem of finding the equilibrium states of a randomly distributed spin system in lattices consisting of $6\times6\times6$ or $10\times10\times10$ and $20\times20\times20$ ions. Figure 5a (solid circles) shows the calculated dependence of the magnetic susceptibility obtained in Ref. 20 for a randomly distributed system of magnetic ions in a body-centered lattice. It can be seen from this figure that if account is taken of the temperature dependence of $\chi_\perp^*(x,T)$, the agreement between the ratio $\chi_\perp^*(x)/\chi_\perp(0)$ calculated at $T=0$ and the experimental magnetic-susceptibility ratio $\chi_\perp^*(x)/\chi_\perp(0)$ at $T=2$ K, obtained in weak magnetic fields, is good. In Fig. 5b are shown the values of magnetic susceptibility $\chi_\perp(x)/\chi_\perp(0)$ for the investigated $Mn_{1-x}Zn_xF_2$ compounds with allowance for the content of the Mn^{++} in each investigated sample. The dark circles in Fig. 5b also represent the calculated $\chi_\perp(x)/\chi_\perp(0)$ dependence obtained in Ref. 20. It can be seen that when M^{++} is accounted in this manner and if $0<x<0.6$, agreement is observed between the experimental and calculated ratios $\chi_\perp(x)/\chi_\perp(0)$, where $\chi_\perp(x)$ is the magnetic susceptibility measured in strong magnetic fields (light circles in Fig. 5b) and does not depend on the temperature. As indicated in Ref. 20, the experimental magnetic susceptibility $\chi_\perp(x)$ in strong magnetic fields at $0<x<0.6$ can be represented by the expression $\chi_\perp(x)\sim(x-x_c)^\tau$, where $\tau = -(0.5\pm0.1)$ and x_c is the concentration in which no phase transition into the ordered state of $Mn_{1-x}Zn_xF_2$ is observed at $T=T_N$. A second distinguishing property of the investigated $M_{1-x}Zn_xF_2$ systems is the onset of a nonlinear dependence of the magnetic moment $M_x(H_x)$ at $\mathbf{H}\perp$ [001] in weak magnetic fields, and of a temperature dependence of the magnetic susceptibility $\chi_\perp^*(T)$ also measured in weak magnetic fields $H\to0$. It should be noted that both the nonlinearity of $M_x(H_x)$ and the $\chi_\perp^*(T)$ dependence manifest themselves most strongly when the concentration x of the Zn^{++} ions approaches x_c, i.e., at $x>0.5$. The nonlinearity of $M_x(H_x)$ at $\mathbf{H}\perp$ [001] and the onset of a ferromagnetic moment $m_\perp$ in $Mn_{1-x}Zn_xF_2$ at $x>0.5$ in weak magnetic fields $H<10$ kOe can be explained on the basis of the data of Ref. 20, in which it is indicated that this nonlinearity of $M_x(H_x)$ and the corresponding increase of $\chi_\perp(T)$ can occur when x approaches x_c, owing to the onset and the fluctuations of the randomly distributed ferromagnetic moment $\mathbf{m}_\perp^i$ which occurs in the (001) plane in dilute antiferromagnets. The appearance of a randomly distributed $\mathbf{m}_\perp^i$ in dilute antiferromagnets is due, according to Eqs. (3), to the local asymmetry of the interactions of the randomly distributed M^{++} ions and because the two sublattices of $M_{1-x}Zn_xF_2$ are not locally compensated. With increasing $\mathbf{H}\perp$ [001], saturation of these ferromagnetic fluctuations takes place along the magnetic field $\mathbf{m}_\perp^i \| \mathbf{H}$, and the $M_x(H_x)$ dependence in weak magnetic fields H becomes nonlinear. Measurement, in weak magnetic fields, of the value $M_\perp = \Sigma_i \mathbf{m}_\perp^i$ that arises at $x>0.5$ (as indicated in Ref. 20), is a characteristic of such fluctuations and of the lack of compensation of the two sublattices when the magnetic ions M^{++} are randomly distributed in the $M_{1-x}Zn_xF_2$ lattice. We succeeded in measuring the $M_\perp(x)$ dependence only for several $Mn_{1-x}Zn_xF_2$. For a more detailed clarification of the indicated phenomena and for an explanation of the role of the fluctuations of the ferromagnetic moment $\mathbf{m}_\perp^i$, which take place in the basal plane (001) when the Zn^{++} ion concentration approaches x_c, additional experiments on a large number of $M_{1-x}Zn_xF_2$ samples are necessary. We note however that for the $Mn_{1-x}Zn_xF_2$ samples investigated by us the $M_\perp(x)$ dependence can be represented by the expression $M_\perp(x)\propto(x-x_c)^{-\alpha}$, where $\alpha = 0.5\pm0.1$. In the present paper we shall assume, in accordance with the conclusions of Refs. 11 and 20, that when the interacting magnetic ions M^{++} are randomly distributed in the equilibrium state of $M_{1-x}Zn_xF_2$, the orientation of the antiferromagnetic vector $\mathbf{L}$ is distributed in a certain interval of angles θ_i relative to the easy magnetization axis of the corresponding antiferromagnet MF_2. The angles θ_i of the orientation of $\mathbf{L}$ are randomly distributed over the $M_{1-x}Zn_xF_2$ lattice, and their value depends on the concentration x of the Zn^{++} ions.

The antiferromagnetic properties of dilute $M_{1-x}Zn_xF_2$ systems turned out to be interesting. In considering these properties we shall assume that when the M^{++} ions are randomly replaced by Zn^{++} in the MF_2 lattice, the investigated system is described, at each concentration x, by the effective average exchange interaction H_E corresponding to the measured temperature T_N and to the measured perpendicular magnetic susceptibility $\chi_\perp$ in strong magnetic fields, by the effective average anisotropic field H_A responsible for the orientation of antiferromagnetic vector $\mathbf{L}$ in the crystal, and by the effective Dzyaloshiskiĭ interaction field $H_D = \sigma_{D_\perp}/\chi_\perp$, which is responsible for the possible onset of the weak ferromagnetism. It must be indicated here that in a dilute antiferromagnet the effective fields are distributed over the crystal in the manner indicated above and with average values H_E, H_A, and H_D. In the Hamiltonian (1), the effective Dzyaloshinskiĭ interaction can be introduced by writing down the single-ion anisotropy invariant in the form

$$-D\sum_{ij}[S_i^x S_i^y - S_j^x S_j^y]p_i p_j, \quad (4)$$

where, just as in (1), $p_i p_j = 1$ if the states i and j are occupied

by the ions M^{++}, $p_i p_j = 0$ in all other cases, and D is the Dzyaloshinskiĭ interaction corresponding to MF_2 for two magnetic ions M^{++} side by side. A rigorous calculation of the magnetic properties of the system $M_{1-x}Zn_xF_2$ would have to be performed on the basis of the Hamiltonian (1) with the interaction (4), but such a calculation is impossible, in the general case and the calculation for sublattices with finite numbers of ions, as in Refs. 11 and 20, entails considerable difficulties and calls for the use of a computer.

In our interpretation of the experimental data we shall use the phenomenological theory developed by I. E. Szyaloshinskiĭ and A. S. Borovik-Romanov[21,22] on the basis of the symmetry of the indicated antiferromagnets MF_2 with the values of H_E, H_A, and H_D, that have been determined by us and characterize the magnetic properties of $M_{1-x}Zn_xF_2$. It must be indicated, however, that this approach is difficult at concentrations close to x_c, where the singularities of the magnetic properties of $M_{1-x}Zn_xF_2$ manifest themselves most strongly.

We shall assume that the magnetic properties of $M_{1-x}Zn_xF_2$ are described by the thermodynamic potential Φ corresponding to MF_2, but with experimentally obtained values of the effective exchange and relativistic interactions. For crystals of tetragonal symmetry $D_{4h}{}^{14}$ the thermodynamic potential that describes the magnetic properties takes the form[22]

$$\Phi = {}^1/_2 B\mathbf{m}^2 + {}^1/_2 D(\boldsymbol{\gamma}\mathbf{m})^2 - e(\gamma_x m_y + \gamma_y m_x) + {}^1/_2 a\gamma_z{}^2 + {}^1/_2 g\gamma_x{}^2\gamma_y{}^2 - 2d(\boldsymbol{\gamma}\mathbf{m})\gamma_x\gamma_y - \mathbf{mH}, \qquad (1')$$

where $\mathbf{m} = \mathbf{M}_1 + \mathbf{M}_2$ is the magnetic vector and $\gamma = (\mathbf{M}_1 - \mathbf{M}_2)/2M_0$ is a unit antiferromagnetic vector. The invariance $Bm^2/2$ and $D(\boldsymbol{\gamma}\mathbf{m})^2/2$, corresponding to exchange and exchange-relativistic interaction in the crystal, determine the perpendicular $\chi_\perp = 1/B$ and the longitudinal $\chi_\parallel = 1/(B+D)$ magnetic susceptibilities of the crystals. The invariants $a\gamma_z^2/2$ and $g\gamma_x^2\gamma_y^2/2$ correspond to the effective anisotropy fields $H_{AE} = (aB)^{1/2}$ and $H^*_{AE} = (gB)^{1/2}$ which are responsible for the orientation of the antiferromagnetic vector in the crystal relative to the tetragonal axis [001] and the binary axis [100]. The invariants $-e(\gamma_x m_x + \gamma_y m_x)$ and $-2d(\boldsymbol{\gamma}\mathbf{m})\gamma_x\gamma_y$ correspond to the Dzyaloshinskiĭ interaction responsible for the transverse $\sigma_{D_\perp} = e/B$ and longitudinal $\sigma_{D_\parallel} = (e+d)/(B+D)$ weak ferromagnetism of the crystals. It must be indicated that in dilute antiferromagnets, strictly speaking, the magnetic vector $\mathbf{m}$ and the unit antiferromagnetic vector $\boldsymbol{\gamma}$ for the unit cell have not been determined, but we shall assume, to preserve the symmetry of the relativistic interactions that $\mathbf{m}$ and $\boldsymbol{\gamma}$ are the mean values of these vectors in the crystal when the two sublattices of $M_{1-x}Zn_xF_2$ are ideally compensated. The sublattices in the investigated single crystals can on the average be regarded as compensated in the entire concentration interval of the Zn^{++} ions except for the concentrations closest to x_c ($0.5 < x < 0.7$), where the indicated characteristic properties of the dilution manifest themselves particularly.

In general form, the calculation of the dependence of the magnetic moment on the applied magnetic field for different orientations of $\mathbf{H}$ relative to the crystal axis was carried out in Refs. 4 and 8 in a description of the magnetic properties and of the weak ferromagnetism of NiF_2 and CoF_2. We consider now specific properties of the investigated $M_{1-x}Zn_xF_2$ samples, and interprets the experiments represented in Figs. 2–9.

1. $Mn_{1-x}Zn_xF_2$

As indicated in Refs. 9 and 11 (see Fig. 2), when the magnetic ions Mn^{++} are replaced by the nonmagnetic Zn^{++} in the MnF_2 crystal lattice a decrease takes place in the magnetic field of the phase transition connected with the flipping of the antiferromagnetic vector $\mathbf{L}$ from the state with orientation of $\mathbf{L}$ close to the [001] axis into the state $\mathbf{L}\perp$ [001] at $\mathbf{H}\parallel$ [001]. At an Zn^{++} ion concentration $x = 0.46$, such a phase transition takes place in a magnetic field $H_c = (42 \pm 2)$ kOe. From Fig. 2, which shows the plots of $M_x(H_x)$ and $M_y(H_x)$, it can be seen that such a phase transition takes place in a certain region of magnetic fields near H_c and is accompanied not by a jumplike flipping of the antiferromagnetic vector $\mathbf{L}$, as in MnF_2, but by a smooth rotation. The effective exchange-interaction field $H_E = M_0/\chi_\perp$, where $\chi_\perp$ is the perpendicular magnetic susceptibility measured in strong magnetic fields and independent of the temperature, is given by $H_E = (200 \pm 20)$ kOe. The average effective anisotropic field H_{AE} responsible for the orientation of antiferromagnetic vector $\mathbf{L}$ in the crystal can be determined from the value of field $H_c = [aB/(1-\chi_\parallel/\chi_\perp)]^{1/2}$ (Ref. 1), if the longitudinal magnetic susceptibility $\chi_\parallel$ is known, namely $H_{AE} = (41 \pm 2)$ kOe. The reason why the phase transition takes place in a certain region of magnetic fields H_c is apparently that in a dilute $Mn_{1-x}Zn_xF_2$ crystal there exists a distribution of the magnetic fields H^*_{AE} with a mean value H_{AE} governed by the randomness of the distribution of the interacting Mn^{++} ions. In this case, as indicated above and in Refs. 9,11 and 12, the antiferromagnetic vector $\mathbf{L}$ is oriented in a certain region of angles θ_i around the [001] axis. The experimental dependences of T_N on the ion concentration x in the $Mn_{1-x}Zn_xF_2$ crystal (see Fig. 4) reflect the effective changes of the exchange interaction in the investigated crystal when the number of interacting ions decreases.

2. $Co_{1-x}Zn_xF_2$

Interesting factors in the investigation of $Co_{1-x}Zn_xF_2$ were found to be the magnetic properties connected with the phase transitions from an antiferromagnetic state with antiferromagnetic vector $\mathbf{L}$ oriented near the tetragonal axis into a weak-ferromagnetism state with an antiferromagnetic vector oriented in the (001) plane. These transitions occur when the magnetic field is oriented along the [100] or [010] axis and are observed in the employed range of fields at concentrations $x > 0.4$. In pure CoF_2, as indicated in Refs. 6 and 7, such phase transitions take place in magentic fields $H_c \approx 120$ kOe at the orientation $\mathbf{H}\parallel$ [100] and in stronger fields 200 kOe at the orientation $\mathbf{H}\parallel$ [001].

As seen from Fig. 6a (curve 1), the phase transition from the antiferromagnetic state into the state with transverse weak ferromagnetism $\sigma_{D_\perp}$ takes place in $Co_{1-x}Zn_xF_2$ when a magnetic field H_c (30 ± 2) kOe with orientation $\mathbf{H}\parallel$ [100] is

applied. In magnetic fields $H > 35$ kOe the $M_x(H_x)$ dependence is described by the expression $M_x(H_x) = \sigma_{D_\perp} + \chi_\perp H$. As indicated in Refs. 6, 13, and 23, it must be assumed that at the orientation $\mathbf{H} \parallel [100]$, owing to the onset of a ferromagnetic moment $\sigma_{D_\perp} \parallel \mathbf{H}$ when the magnetic field is increased from 0 to 30 kOe, the antiferromagnetic vector **L** rotates in the (100) plane from an orientation close to the [001] axis into an orientation $\mathbf{L} \parallel [010]$. This rotation terminates at a magnetic field value $H_c \approx 30$ kOe. The rotation of the antiferromagnetic vector **L** in the (001) plane at an orientation $\mathbf{H} \parallel [100]$ terminates in a certain magnetic-field region near H_c, this being due to the random distribution about the mean values of the effective fields H_E, H_{AE}, and H_D owing to the random location of the interacting Co^{++} ions. Calculation of the magnetization curve $M_x(H_x)$ at $\mathbf{H} \parallel [100]$ on the basis of the thermodynamic potential (1) was carried out in Ref. 6. This dependence is of the form

$$M_x(H_x) = \sigma_D \sin\theta + \chi_\perp H,$$

where θ is the angle of rotation of the antiferromagnetic vector **L** and is reckoned from the [001] axis. Substituting the expression for $\sin\theta$ in the expression for the function $M_x(H_x)$, we can draw a theoretical curve for the values of H_E, H_{AE} and $H_{D_\perp}$ obtained by us. Agreement is observed between the calculated $M_x(H_x)$ dependence and the experimental one. The small discrepancy between the theoretical $M_x(H_x)$ dependence and the experimental one near the phase-transition point H_c is due to the randomness of the distribution of the Co^{++} ions. Knowing the value of $\sigma_{D_\perp}$ and of $\chi_\perp$ of the investigated $Co_{1-x}Zn_xF_2$, we can obtain the effective Dzyaloshinkiĭ field $H_{D_\perp} = (46 \pm 4)$ kOe responsible for the transverse weak ferromagnetism. At a magnetic-field orientation $\mathbf{H} \parallel [001]$, in the investigation of $Co_{1-x}Zn_xF_2$ ($x = 0.5$), we observe, just as in the investigation of $Mn_{1-x}Zn_xF_2$ phase transition due to the rotation of the antiferromagnetic vector **L** from a state with **L** close to the [001] axis into a state with $\mathbf{L} \perp [001]$ (Fig. 6a, curve 3). According to the investigations of $M_x(H_x)$ (Fig. 6a, curve 3) and $M_y(H_x)$ (Fig. 6c, curve 1) at $\mathbf{H} \parallel [001]$, the phase transition takes place in a certain region of magnetic fields near H_c. The values of the effective fields H_E, H_{AE} and H_D, of the phase-transitions fields H_c and H_c^*, and of the magnetic susceptibilities $\chi_\perp$ and $\chi_\parallel$ are connected, as found by calculations[11] based on the thermodynamic potential, by the relation

$$H_c H_{D\perp} = (1 - \chi_\parallel/\chi_\perp) H_c^{*2} - H_D^2.$$

This relation, at the values obtained by us for the parameters contained in it, is accurate to within 10%. In Ref. 8, in an investigation of weak ferromagnetism of CoF_2, it was indicated that at the orientation $\mathbf{H} \parallel [110]$ of the magnetic vector **L** in the $(1\bar{1}0)$ plane, a state arises with a longitudinal weak ferromagnetism $\sigma_{D_\parallel} \parallel \mathbf{L}$, but to investigate this state in pure CoF_2, it is necessary to have magnetic fields **H** stronger than 200–300 kOe. A decrease of the effective fields H_E and H_{AE} in the system $Co_{0.5}Zn_{0.5}F_2$ has enabled us to investigate, this state in greater detail in the employed magnetic fields. In the investigation of the dependences of the three components of the magnetic moment $M(H)$ of $Co_{0.5}Zn_{0.5}F_2$ (Fig. 6, curves 1–3) in a magnetic field oriented along the binary axis [110], we can likewise state that with increasing H, just as in CoF_2 (Ref. 8), the antiferromagnetic vector **L** begins to rotate away from the [001] axis in the (110) plane. At this rotation of **L** (Fig. 6c, curve 2), a state is produced with a magnetic moment $M_x(H_x)$ that characterizes the onset of longitudinal weak ferromagnetism σ_D, oriented along the rotating antiferromagnetic vector **L** and the onset of a transverse weak ferromagnetism $\sigma_{D_\parallel}$ oriented perpendicular to the rotating antiferromagnetic vector **L**. The equations of the rotation of **L** at this orientation of **H**, as functions of the three components of the mangetic moment $M(H)$, were obtained in Ref. 8. In weak magnetic fields H, the functions $M(H)$ can be represented in the form

$$M_x(H_x) = \sigma_{D\perp} \sin\theta - (\sigma_{D\perp} - \sigma_{D\parallel}) \sin^3\theta,$$
$$M_z(H_x) = -(\sigma_{D\perp} - \sigma_{D\parallel}) \sin^2\theta \cos\theta. \quad (5)$$

As can be seen from (5), when **L** is rotated in the $(1\bar{1}0)$ plane a longitudinal weak ferromagnetism $\sigma_{D_\parallel}^* = \sigma_{D_\parallel} \sin^2\theta$ and a transverse weak ferromagnetism $\sigma_{D_\perp}^* = \sigma_{D_\perp} \sin\theta \cos\theta$ are produced. Calculation of the magnetization curves $M_x(H_x)$ at $\mathbf{H} \parallel [110]$ (Ref. 8) and at the indicated values of $H_{D_\perp}, H_{AE}, \chi_\perp, \chi_\parallel$ and $\sigma_{D_\perp}$ for $Co_{1-x}Zn_xF_2$ has shown that the longitudinal weak ferromagnetism is $\sigma_{D_\parallel} = (720 \pm 50)$ kOe.

The constant value of $M_z(H_x)$ that does not depend on the field H (Fig. 6d, curve 2) at $\mathbf{H} \parallel [110]$ corresponds to an increase of the magnetic moment $M_z(H_x) = \sqrt{2}(\sigma_{D_\perp} - \sigma_{D_\parallel})/4$ and to a maximum rotation angle $\theta \approx 45°$ in the $(1\bar{1}0)$ plane. With further increase of **H**, rotation of the antiferromagnetic vector **L** takes place from the $(1\bar{1}0)$ plane towards a direction perpendicular to **H**. This rotation is characterized by the onset of a magnetic moment $M_y(H_x)$ and by decrease of $M_z(H_x)$ (see Fig. 6c and 6d, curves 4–7). In our experiments, these become most pronounced when the applied magnetic field **H** is oriented at a certain small angle ψ to the $[1\bar{1}0]$ axis (Fig. 6d, curve 4), when the rotation of **L** from the $(1\bar{1}0)$ plane takes place in weaker magnetic fields because of the onset of a transverse weak ferromagnetism in the plane $\sigma_{D_\perp} \parallel [100]$ or $\sigma_{D_\perp} \parallel [010]$. The value of the effective Dzyaloshinskiĭ-interaction field responsible for the longitudinal weak ferromagnetism $\sigma_{D_\parallel}$ turned out to be $H_{D_\parallel} = \sigma_{D_\parallel}/\chi_\parallel = (70 \pm 10)$ kOe, while the auxiliary effective field was $H_D^* = \sigma_{D_\parallel}/\chi_\perp = (23 \pm 3)$ kOe. The ratio $\sigma_{D_\parallel}/\sigma_{D_\perp}$ of the ferromagnetic moments for the measured $Co_{1-x}Zn_xF_2$ agrees fully with the ratio obtained in Ref. 8 from a calculation of the magnetization curves $M_x(H_x)$ and $M_z(H_x)$ at $\mathbf{H} \parallel [110]$. At the values of $\sigma_{D_\perp}$ and $\sigma_{D_\parallel}$ obtained by us it can be seen that a large contribution is made to the magnetic moment $M_z(H_x)$ (Fig. 6d, curve 2) at $\mathbf{H} \parallel [110]$ by the weak longitudinal ferromagnetism. The dash-dot line in Fig. 6d shows the function $M_z(H_x)$ if it is assumed that $\sigma_{D_\parallel} = 0$. The randomness of the distribution of the Co^{++} ions in $Co_{1-x}Zn_xF_2$ when measuring the components $M_z(H_x)$ and $M_y(H_x)$ possibly affects the character of these curves at $x > 0.5$ in weak magnetic fields $H < 5$ kOe, where a perpendicular component $\mathbf{m}_\perp^i$ of the mag-

netic-moment vector $\mathbf{M}_i$ appears for each of the Co^{++} ions, and the sublattices are not locally compensated. In magnetic fields H stronger than 3–5 kOe, as the concentration x approaches x_c, when the perpendicular component $\mathbf{m}_\perp^i$ of the magnetic moments of the Co^{++} ions is magnetized along the magnetic field $\mathbf{H}$, this magnetic moment makes no contribution to $M_y(H_x)$ and $M_z(H_x)$, and contributes only to $M_x(H_x)$, giving a ferromagnetic moment $m_\perp$. In the $Co_{0.5}Zn_{0.5}F_2$ investigated by use we have $m_\perp \ll \sigma_{D_\perp}$. As the concentration x approaches x_c, this value of $m_\perp$ increases just as in $Mn_{1-x}Zn_xF_2$; also increasing in this case is the temperature depenence of $\chi_\perp^*(T)$ in weak magnetic fields, but for a more detailed investigation of this phenomenon we need additional experiments at concentrations close to x_c.

3. $Ni_{1-x}Zn_xF_2$

In investigation of the three magnetic-monent components $M_x(H_x)$, $M_y(H_x)$ and $M_z(H_x)$ for $Ni_{1-x}Zn_xF_2$ ($x = 0.5$) we have observed (see Fig. 8a, curve 1) that when the magnetic field is oriented in the basal plane (001) in weak magnetic fields, and at the $\mathbf{H}\|$ [100] orientation in the entire range of employed magnetic fields, the single crystal $Ni_{1-x}Zn_xF_2$ has a weak ferromagnetism $\sigma_{D_\perp}$, with $\sigma_{D_\perp}\|$ [100] or $\sigma_{D_\perp}\|$ [010]. At the orientation $\mathbf{H}\|$ [100] the $M_x(H_x)$ dependence is described by the expression $M_x(H_x) = \sigma_{D_\perp} + \chi_\perp H$. The antiferromagnetic vector $\mathbf{L}$ is oriented along the [010] axis and $\mathbf{L} \perp \mathbf{H}$. Knowing the values of the ferromagnetism $\sigma_{D_\perp}$ and of the transverse magnetic susceptibility $\chi_\perp$, it is possible to obtain the effective Dzyaloshinskiĭ field responsible for the onset of weak ferromagnetism: $H_D = (8.5 \pm 0.5)$ kOe. Knowing the magnetic susceptibility $\chi_\perp$ obtained in strong magnetic fields, we can determine the exchange-interaction effective field $H_E = (400 \pm 40)$ kOe. At an applied-magnetic-field oreintation $\mathbf{H}\|$ [110] (Fig. 8a), just as in the investigation of NiF_2 (Fig. 8b) we observed a rotation of the antiferromagnetic vector $\mathbf{L}$ from a state with $\mathbf{L}\|$ [100] or $\mathbf{L}\|$ [010] into a state with $\mathbf{L}\|$ [$1\bar{1}0$], perpendicular to $\mathbf{H}$. In weak magnetic field H the dependence $M_x(H_x)$ can be described in this case by the expression $M_x(H_x) \approx \sqrt{2}\sigma_{D_\perp}/2 + \chi_\perp^* H$, and when the magnetic field is increased $M_x(H_x)$ approaches asymptotically $M_x(H_x) = \chi_\perp H$. In magnetic fields $H > 40$ kOe, the experimental $M_x(H_x)$ dependence practically coincides with the relation $M_x(H_x) = \chi_\perp H$. From the experiment illustrated in Fig. 8a (curve 2) we can deduce that in magnetic fields $H > 40$ kOe, at an oreintation $\mathbf{H}\|$ [110], the antiferromagnetic vector $\mathbf{L} \perp \mathbf{H}$ and in this case there is no transverse weak ferromagnetism, $\sigma_{D_\perp} = 0$. The state with $\mathbf{L}\|$ [$1\bar{1}0$], as indicated by Dzyaloshinskiĭ[22] and as shown by an investigation[4] of NiF_2, is characterized by the onset of a longitudinal weak ferromagnetism $\boldsymbol{\sigma}_{D_\|}\|\mathbf{L}$. Figure 8c (curve 1) shows the dependence of the magnetic moment $M_y(H_x)$, measured perpendicular to the applied magnetic field, along the [$1\bar{1}0$] axis at $\mathbf{H}\|$ [110]. Curve 2 of the same figure shows the $M_y(H_x)$ dependence at $\mathbf{H}\|$ [100]. It can be seen from this figure that at the orientation $\mathbf{H}\|$ [100] the $M_y(H_x)$ component is close to zero at $H > 3$–4 kOe. The nonzero magnetic moment $M_y(H_x)$ at $\mathbf{H}\|$ [100] in weak magnetic fields, as indicated in Ref. 4, is connected with the presence in $Ni_{1-x}Zn_xF_2$ of a domain structure of the ferromagnetic moment $\sigma_{D_\perp}$. At a magnetization $\boldsymbol{\sigma}_{D_\perp}\|\mathbf{H}\|$ [100] and in magnetic fields $H > 5$ kOe we have $M_y(H_x) \approx 0$; the $M_y(H_x)$ component is close to zero also when $\mathbf{H}$ makes small angles $\psi \approx 5°$ with the [100] axis. At a strict magnetic field orientation $\mathbf{H}\|$ [110], $M_y(H_x)$ is also close to zero in the entire range of magnetic fields H, but when $\mathbf{H}$ is oriented at an angle $\psi \approx 1$–2° to the [110] axis, a considerable magnetic moment $M_y(H_x)$ appears (curve 2, Fig. 8c). The magnetic moment $M_y(H_x)$ tends with increasing magnetic field H to a constant value that does not depend at $H > 40$ kOe on the small angle ψ, and $M_y(H_x) = \sigma_{D_\|}$. The measured value of $M_y(H_x)$ is the ferromagnetic moment directed along the [$1\bar{1}0$] axis at the orientation $\mathbf{H}\|$ [110]. This ferromagnetic moment is directed along the flipped antiferromagnetic vector $\mathbf{L}$. According to Dzyaloshinskiĭ,[22] this quantity is the longitudinal weak ferromagnetism $\boldsymbol{\sigma}_{D_\|}\|\mathbf{L}$. In an investigation[4] of NiF_2 at $\mathbf{H}\|$ [110] we have also observed a rotation of the antiferromagnetic vector $\mathbf{L}$ from $\mathbf{L}\|$ [100] into $\mathbf{L}\|$ [$1\bar{1}0$]. In NiF_2, however, the appreciable effective anisotropy field in the (001) plane has kept us from obtaining, in the employed range of magnetic fields up to 65 kOe, a state with longitudinal weak ferromagnetism $\sigma_{D_\|}$ in pure form. Replacing in the NiF_2 lattice the magnetic Ni^{++} ions by the nonmagnetic Zn^{++} ions, we decreased effectively the exchange interaction H_E of the Ni^{++} ions and the anisotropy field H_{AE} in the basal plane (001), and it is this which enables us in the employed range of magnetic fields H up to 65 kOe at $\mathbf{H}\|$ [110], to turn the antiferromagnetic vector $\mathbf{L}$ along the [$1\bar{1}0$] axis and to observe a state with longitudinal weak ferromagnetism $\boldsymbol{\sigma}_{D_\|}\|\mathbf{L}$. In an investigation[4] of NiF_2 we obtained, on the basis of the thermodynamic potential (1), an equation for the rotation of the antiferromagnetic vector $\mathbf{L}$ at $\mathbf{H}\|$ [110], and expression for the magnetic moments $M_x(H_x)$ and $M_y(H_x)$ under this rotation. Knowing the deformation moment $\sigma_{D_\|}$ we can obtain the effective Dzyaloshinskiĭ field responsible for the onset of $\sigma_{D_\|}$, namely $H_{D_\|} = (18 \pm 2)$ kOe, and the auxiliary field $H_D^* = \sigma_{D_\|}/\chi_\perp = (3 \pm 0.2)$ kOe. The longitudinal magnetic susceptibility can be determined, just as in Ref. 4, from experimental study of $M_x(H_x)$ at $\mathbf{H}\|$ [110] in weak fields $H < 5$ kOe. In this case the measured magnetic susceptibility is $\chi_\perp^* = (\chi_\perp + \chi_\|)/2$. The maximum rotation angle φ of $\mathbf{L}$ away from the [100] axis, calculated at the obtained numerical values of H_E, $H_{D_\perp}$, $H_{D_\|}$, $H_{D\|}^*$, $\chi_\perp$ and $\chi_\|$ and at the effective anisotropy field H_{AE} in the plane, $H_{AE} = (200 \pm 30)$ kOe, amounts to $\sim 40°$. Curve 2 of Fig. 9 shows the dependence of the ferromagnetic moment $\sigma_{D_\|}(T)$ on the temperature. The more rapid decrease of $\sigma_{D_\|}(T)$ with increasing temperature is apprently due to the temperature dependence of the terms in the expression for $\sigma_{D_\|} = (e + dL^3)/(B + DL^2)$ compared with $\sigma_{D_\perp} = eL/B$. At a temperature $T > 18°$, the $M_x(H_x)$ dependence is determined by the expression $M_x(H_x) = \sigma + \chi H$ and does not depend on the orientation of $\mathbf{H}$ in the (001) plane, in which case $M_y(H) = 0$. Just as in Ref. 4, in an investigation of NiF_2 at temperatures $T > 18$ K and $\mathbf{H}\|$ [100], a

state is observed with transverse or weak ferromagnetism $\sigma_{D_\perp}(T)\|\mathbf{H}$, and at $\mathbf{H}\|$ [110] a state is observed with longitudinal weak ferromagnetism $\sigma_{D_\parallel}(T)\|\mathbf{H}$. In this case $\sigma_{D_\perp}(T) = \sigma_{D_\parallel}(T)$.

Just as for $Mn_{1-x}Zn_xF_2$ and $Co_{1-x}Zn_xF_2$, an increase of the magnetic susceptibility in weak magnetic fields as a function of temperature is observed in $Ni_{1-x}Zn_xF_2$ (Fig. 9b, curves 1 and 2). This increase, however, is not as appreciable as observed in $Mn_{1-x}Zn_xF_2$ as the concentration x approaches x_c. It is difficult to observe the nonlinearity of the magnetization $M_x(H_x)$ at $\mathbf{H}\perp$ [001] in the investigated $Ni_{1-x}Zn_xF_2$, since this nonlinearity is determined mainly by the onset of weak ferromagnetism $Ni_{1-x}Zn_xF_2$, but apparently just as in $Co_{1-x}Zn_xF_2$, at $x = 0.5$ in $Ni_{1-x}Zn_xF_2$ we have $m_\perp \ll \sigma_{D_\perp}$, as is confirmed by the experiment illustrated in Fig. 8 by curve 2. The $M_x(H_x)$ dependence at $\mathbf{H}\|$ [110] in strong magnetic fields is determined by the expression $M_x(H_x) = \chi_\perp H$.

Thus, we have shown that when the ions M^{++}($M = Mn^{++}$, Co^{++}, Ni^{++}) in MF_2 are randomly replaced by Zn^{++} ions, the dilute antiferromagnetic $M_{1-x}Zn_xF_2$, at a Zn^{++} ion concentration $0 < x < 0.5$, have the properties of the corresponding antiferromagnets MF_2 but with smaller values of the temperature T_N, of the phase transition into the disordered state, of the effective exchange interaction field H_E of the anisotropic field H_{AE} responsible for the orientation of the antiferromagnetic vector $\mathbf{L}$ relative to the crystal axis, and of the Dzyaloshinskiĭ field responsible for the onset of the transverse $\sigma_{D_\perp}$ and of the longitudinal $\sigma_{D_\parallel}$ weak ferromagnetism. A decrease of the anisotropy fields responsible for the orientation of the antiferromagnetic vector $\mathbf{L}$ in the crystals makes it possible to observe in $Mn_{1-x}Zn_xF_2$ phase transitions connected with the weak ferromagnetism in weaker magnetic fields compared with the corresponding MF_2. Distinguishing features of the dilute antiferromagnets $Mn_{1-x}Zn_xF_2$ are the growth of the perpendicular magnetic susceptibility, measured in weak magnetic fields with decreasing temperature $T < T_N$, and the onset of a nonlinear $M_x(H_x)$ dependence at $\mathbf{H}\perp$ [001]. These features manifest themselves most strongly as the concentration x of the Zn^{++} ions approaches x_c. The observed distinguishing properties are determined by the onset of a perpendicular component $\mathbf{m}_\perp^i$ of the magnetic moment $\mathbf{M}_i$ of the M^{++} ion in the plane (001), randomly distributed in the crystal lattice. In $Mn_{1-x}Zn_xF_2$ and $Co_{1-x}Zn_xF_2$ at $\mathbf{H}\|$ [001] we investigated the phase transitions connected with the rotation of antiferromagnetic vector $\mathbf{L}$ in the (001) plane, and in $Co_{1-x}Zn_xF_2$ at $\mathbf{H}\|$ [100] we investigated the phase transition from the antiferromagnetic state into a state with transverse weak ferromagnetism $\sigma_{D_\perp}$. In $Co_{1-x}Zn_xF_2$ and $Ni_{1-x}Zn_xF_2$ at $\mathbf{H}\|$ [110] we investigated the phase transitions accompanied by the onset of a longitudinal weak antiferromagnetism $\sigma_{D_\parallel}$. In the absence of a magnetic field, the single-crystal $Ni_{1-x}Zn_xF_2$ is a weak ferromagnet.

The authors thank P. L. Kapitza for interest in the work, A. S. Borovik-Ramanov for directing the work, and I. E. Dzyaloshinskiĭ for a discussion of the results.

[1)]In the determination of the numerical values of the magnetic susceptibilities $\chi(x)$, where x is the content of the Zn^{++} ions in $Mn_{1-x}Zn_xF_2$, error was made in Ref. 9 in the allowance for the content of these ions. The values of the magnetic susceptibilities $\chi(x,T)$ shown in Fig. 2, and of the magnetic moments $M(x,H)$ from Fig. 1, should be increased by a factor $1/x$. This yields the true values of the magnetic moments and of the magnetic susceptibilities for $Mn_{1-x}Zn_xF_2$.

[1]L. M. Maltaresse and J. W. Staut, Phys. Rev. 94, 1792 (1954).
[2]S. Foner, Proc. Internat. Conf. on Magn., Nottingham, 1964, p. 438.
[3]R. Joenk and R. M. Bozoerth, *ibid.* (no page given).
[4]A. S. Borovik-Romanov, A. N. Bazhan, and N. M. Keĭnes, Zh. Eksp. Teor. Fiz. **64**, 1367 (1973) [Sov. Phys. JETP **37**, 695 (1973)].
[5]L. V. Velikov, L. A. Prozorova, A. S. Prokhorov, E. G. Rudashevskiĭ, and A. I. Smirnov, Zh. Eksp. Teor. Fiz. **68**, 1145 (1975) [Sov. Phys. JETP **41**, 567 (1975)].
[6]K. G. Gurtovoĭ, A. S. Lagutin, and V. I. Ozhogin, *ibid.* **83**, 1941 (1982) [**56**, 1122 (1982)].
[7]V. I. Ozhogin, Candidate's dissertation, Kurchatov Atomic Energy Inst., 1965.
[8]A. N. Bazhan and Ch. Bazan, Zh. Eksp. Teor. Fiz. **69**, 1768 (1975) [Sov. Phys. JETP **42**, 898 (1975)].
[9]A. N. Bazhan and S. V. Petrov, *ibid.* **80**, 669 (1981) [**53**, 337 (1981)].
[10]A. N. Bazhan, S. V. Petrov, and Ya. Ali Amin, Pis'ma Zh. Eksp. Teor. Fiz. **34**, 90 (1981) [JETP Lett. **34**, 85 (1981)].
[11]A. R. King and V. Jaccarino, J. Appl. Phys. **52**, 1785 (1981).
[12]D. P. Balander, A. R. King, and V. Jaccarino, Phys. Rev. Lett. **48**, 1050 (1982).
[13]H. Yshizava, R. J. Birgeneau, H. J. Cugenheim, and H. Skeda, Phys. Rev. Lett. **48**, 438 (1982).
[14]A. N. Bazhan, A. S. Borovik-Romanov, and N. M. Kreĭnes, Prib. Tekh. Eksp. NO. 1,213 (1973).
[15]N. N. Mikhaĭlov and S. V. Petrov, Kristallografiya **11**, 443 (1966) [Sov. Phys. Crystallogr. **11**, 390 (1966)].
[16]S. Z. Petrov and Yu. F. Orekhov, Neorgan, Khim. **27**, 750 (1982).
[17]S. Foner, Proc. Internat. Conf. on Magn., Nottingham, 1964, p. 440.
[18]A. S. Borovik-Romanov, Doctoral dissertation, Inst. Phys. Problems USSR Acad. Sci, 1959.
[19]D. J. Breed, K. Gilijamse, J. W. E. Sternberg, and A. R. Midema, J. Appl. Phys. **41**, 1267 (1970).
[20]A. Brooks Harris and S. Kirkpatric, Phys. Rev. Lett **16**, 542 (1977).
[21]A. S. Borovik-Romanov in: Itogi nauki (Science Summaries), Ya. G. Dorfman, ed., Izd. AN SSSR, 1962, p. 7.
[22]I. E. Dzyaloshinskiĭ, Zh. Eksp. Teor. Fiz. **33**, 1454 (1957) [Sov. Phys. JETP **6**, 1120 (1958)].
[23]N. M. Kreines, *ibid.* **40**, 762 (1961) [**13**, 534 (1961)].

Translated by J. G. Adashko